JOURNAL OF SOLID STATE CHEMISTRY **141,** 424–436 (1998)
ARTICLE NO. SC987969

A Calorimetric Study of the Lanthanide Aluminum Oxides and the Lanthanide Gallium Oxides: Stability of the Perovskites and the Garnets

Yasushi Kanke*,[1] and Alexandra Navrotsky†,[2]

*National Institute for Research in Inorganic Materials, 1-1 Namiki, Tsukuba, Ibaraki 305-0044, Japan; and
†Princeton Materials Institute and Department of Geosciences, Princeton University, Princeton, New Jersey 08544

Received November 7, 1997; in revised form July 16, 1998; accepted July 23, 1998

High-temperature solution calorimetry using a $2PbO \cdot B_2O_3$ solvent at 977 K was performed for $LnMO_3$ perovskites and $Ln_3M_5O_{12}$ garnets (Ln = La–Lu, Y; M = Al, Ga), α-Al_2O_3, and β-Ga_2O_3. The following four reactions were discussed from the viewpoint of thermodynamic parameters, ΔH, ΔS, and ΔV; $LnMO_3 = \frac{1}{5}Ln_3M_5O_{12} + \frac{1}{5}Ln_2O_3$, $Ln_3M_5O_{12} = 3LnMO_3 + M_2O_3$, $\frac{1}{2}Ln_2O_3 + \frac{1}{2}M_2O_3 = LnMO_3$, and $\frac{3}{2}Ln_2O_3 + \frac{5}{2}M_2O_3 = Ln_3M_5O_{12}$. The stability of $LnMO_3$ against the disproportionation to garnet plus sesquioxide is controlled almost entirely by ΔH and $P\Delta V$ but not by $T\Delta S$. On the contrary, the stability of $Ln_3M_5O_{12}$ against disproportionation to perovskite plus sesquioxide is controlled not only by ΔH and $P\Delta V$ but also by $T\Delta S$. The P–T boundary between $Ln_3M_5O_{12}$ and $3LnMO_3 + M_2O_3$ has a negative slope. The positive ΔS and negative ΔV for the disproportionation are caused by an increase in coordination number and an *increase* in bond distance. ΔH of perovskite formation is mainly controlled by two factors, the strengthening of the ionic bond in Ln_2O_3 with decreasing ionic radius of Ln^{3+} and the *weakening* of the ionic bond between Ln and the distant four O atoms in $LnMO_3$ with decreasing ionic radius of Ln^{3+}. ΔH of garnet formation is mainly controlled by two factors, the strengthening of the ionic bond in Ln_2O_3 with decreasing ionic radius of Ln^{3+} and the deviation of the ionic radius of Ln^{3+} from the optimum size for the garnet structure. ΔS values of both perovskite formation and garnet formation are deduced to be negative, which suggests that Ln_2O_3 phases possess relatively large entropies. © 1998 Academic Press

INTRODUCTION

Ln^{3+}–M^{3+}–O binary oxides (Ln = lanthanide; M^{3+} = Al^{3+} (d^0), Ti^{3+}–Fe^{3+} (d^1–d^5), Ga^{3+} (d^{10})) show interesting properties such as optical transparency (perovskites and garnets: M = Al, Ga), magnetism (perovskites: M = Ti, V, Mn; garnets: M = Fe), or high electrical conductivity at high temperatures (perovskites: M = Cr). $Y_3Al_5O_{12}$ is a well-known laser host material. Nd^{3+}-doped $YAlO_3$ and Cr^{3+}-doped $Gd_3(Ga, Sc)_2Ga_3O_{12}$ are potential candidates for laser materials (1, 2). $LaTiO_3$ shows a metal–insulator transition and antiferromagnetism (T_N = 125 K) (3). $La_{1-x}Sr_xVO_3$ is metallic with $x > 0.225$ and is insulating with $x < 0.225$ (4). Perovskitelike $La_{2/3}Ba_{1/3}MnO_x$ shows giant negative magnetoresistance (5). $Y_3Fe_5O_{12}$ and $LaCrO_3$ are well-known magnetic and electric heater materials, respectively. The properties of the binary oxides are influenced by crystal structure. The binary oxides with larger Ln^{3+} (Ln = La–Nd) prepared by solid-state reaction at ambient pressure are perovskites for all M ions (Table 1) (6–9). With decreasing size of Ln^{3+}, however, the oxides crystallize in various structure types at ambient pressure depending on M as follows: no perovskites but $Ln_4M_2O_9$-type phases and garnets (M = Al, Ga) (6, 10), exclusively perovskites independent of Ln^{3+} (M = Ti, V, Cr) (6–8), no perovskites but $LuMnO_3$-type structure (M = Mn) (11), and both perovskites and garnets (M = Fe) (6) (Table 1).

Ideal perovskites, ABO_3, are cubic and consist of twelve-coordinated A atoms and octahedrally six-coordinated B atoms. The A and O atoms form face centered cubic type close-packed layers. However, the perovskites in the Ln^{3+}–M^{3+}–O binary oxide systems are distorted into trigonal ($LnAlO_3$: Ln = La–Nd) (6) or orthorhombic $GdFeO_3$-type (12) symmetries ($LnAlO_3$: Ln = Sm–Lu, Y (6); $LnVO_3$: Ln = La (13), Pr–Lu, Y (8); $LnMO_3$: Ln = La–Lu, Y, M = Ti, Cr, Mn, Ga). The distortion of the M coordination octahedra is small and is almost independent of Ln. In contrast, the distortion of the Ln coordination polyhedra is large and increases with decreasing ionic radius of Ln (14). As distortion increases, the twelve O atoms surrounding a Ln atom separate into two types, eight first-nearest and four second-nearest O atoms. The difference between the mean Ln–O distance for the first-nearest O atoms and the

[1] To whom correspondence should be addressed. E-mail: kanke@nirim.go.jp.
[2] Present address: Department of Chemical Engineering and Materials Science, University of California at Davis, Davis, CA 95616.

0022-4596/98 $25.00

TABLE 1
Ln^{3+}–M^{3+}–O Double-Oxide Systems (Ln = Lanthanide; M = Al, Ti, V, Cr, Mn, Fe, Ga) Observed at Ambient Pressure[a]

	Al	Ti	V	Cr	Mn	Fe	Ga
La	P	P	P	P	P	P	P/M
Pr	P	P	P	P	P	P	P/M
Nd	P	P	P	P	P	P	P/M/G
Sm	P/M	P	P	P	P	P/G	M/G
Eu	P/M	P	P	P	P	P/G	M/G
Gd	P/M/G	P	P	P	P	P/G	M/G
Tb	P/M/G	P	P	P	P	P/G	G
Dy	P/M/G	P	P	P	P	P/G	G
Y	P/M/G	P	P	P	H	P/G	G
Ho	M/G	P	P	P	H	P/G	G
Er	M/G	P	P	P	H	P/G	G
Tm	M/G	P	P	P	H	P/G	G
Yb	M/G	P	P	P	H	P/G	G
Lu	M/G	P	P	P	H	P/G	G

[a] P: perovskite, $LnMO_3$. M: 2/1 phase, $Ln_4M_2O_9$. G: garnet, $Ln_3M_5O_{12}$. H: $LuMnO_3$-type phase, $LnMO_3$.

mean Ln–O distance for the second-nearest O atoms increases with decreasing ionic radius of Ln (14). The $Ln_4M_2O_9$ phases do not have a close-packed array of oxygen atoms and consist of seven-coordinated and octahedrally six-coordinated Ln cations and tetrahedrally four-coordinated M cations (10). The garnets are also not close-packed structures and comprise eight-coordinated Ln^{3+}, octahedrally six-coordinated M^{3+}, and tetrahedrally four-coordinated M^{3+}. The $LuMnO_3$-type phases consist of seven-coordinated Ln^{3+} and five-coordinated M^{3+} cations (11). If distortion is disregarded, Ln and O atoms in the $LuMnO_3$-type phases would form close-packed layers.

Stability of the binary oxides is influenced by both temperature and pressure. Shishido *et al.* (15) synthesized $Gd_3Al_5O_{12}$ by heating a stoichiometric amorphous sample at 1573 K for 1 h in air, followed by rapid quenching. $Gd_3Al_5O_{12}$ decomposed into $3GdAlO_3 + \alpha\text{-}Al_2O_3$ after being maintained at 1773 K for 24 h in air (15). Geller *et al.* (16) prepared $LnGaO_3$ perovskites (Ln = Sm–Er), which had not been obtained by solid-state reaction, by quenching molten mixtures of Ln_2O_3 and Ga_2O_3. The molten state was kept at temperatures ranging from approximately 1923 K for $SmGaO_3$ to approximately 2273 K for $ErGaO_3$ for about 10 min and then quenched. The $LnGaO_3$ perovskites were obtained as a single phase except for $HoGaO_3$ and $ErGaO_3$. Dernier *et al.* (17) obtained $LnAlO_3$ perovskites (Ln = Ho–Lu) by high-pressure synthesis at 3.25 GPa and 1473 ± 10 K. Marezio *et al.* (18, 19) synthesized $LnGaO_3$ perovskites (Ln = Sm–Lu, Y) at 7 GPa and 1273 K or at 4.5 GPa and 1273 K. Al garnets and Ga garnets disproportionate into corresponding perovskites and M_2O_3 phases under high pressure.

The P–T stability of a phase is governed by its free energy. For a given reaction, the free energy change at a given pressure and temperature, $\Delta G(P, T)$ is given by

$$\Delta G(P, T) = \Delta H^\circ - T\Delta S^\circ + \int_{1\text{ atm}}^{P} \Delta V \mathrm{d}P, \qquad [1]$$

where ΔH° and ΔS° are the enthalpy and entropy change at 1 atm and the reference temperature, and the P–V integral reflects the effect of pressure. Several reactions govern the thermodynamic stability of these phases. Their formation from the oxides is given by

$$\tfrac{1}{2}Ln_2O_3 + \tfrac{1}{2}M_2O_3 = LnMO_3 \qquad [2]$$

$$\tfrac{3}{2}Ln_2O_3 + \tfrac{5}{2}M_2O_3 = Ln_3M_5O_{12}. \qquad [3]$$

The relation of garnet and perovskite is controlled by possible disproportionation reactions

$$LnMO_3 = \tfrac{1}{5}Ln_3M_5O_{12} + \tfrac{1}{5}Ln_2O_3 \qquad [4]$$

$$LnMO_3 = \tfrac{1}{7}Ln_3M_5O_{12} + \tfrac{1}{7}Ln_4M_2O_9 \qquad [5]$$

$$Ln_3M_5O_{12} = 3LnMO_3 + M_2O_3. \qquad [6]$$

Furthermore, for M = Fe, oxidation–reduction reactions can be considered.

$$\tfrac{1}{2}Ln_2O_3 + \mathrm{Fe} + \tfrac{3}{4}O_2 = LnFeO_3 \qquad [7]$$

$$\tfrac{3}{2}Ln_2O_3 + 5\mathrm{Fe} + \tfrac{15}{4}O_2 = Ln_3Fe_5O_{12}. \qquad [8]$$

Katsura *et al.* (20) and Kimizuka *et al.* (21) studied the temperature dependence of the standard free energy change, ΔG°, for reactions [7] and [8] by controlling oxygen partial pressure at temperatures 1273–1523 K. They discussed the ΔG° values from the viewpoint of tolerance factors and Madelung energies. To analyze the stability of the perovskites and the garnets as a function of temperature, it is more informative to discuss ΔH and ΔS separately rather than ΔG. The ΔH and ΔS parameters for reactions [2], [3], [4], and [6] with M = Fe can be calculated on the basis of Refs. (21) and (22). The calculated parameters shown in Tables 2 and 3, however, include significant errors, arising largely from uncertainties in determining the temperature dependence of reactions [7] and [8]. It would be advantageous to have direct measurements of ΔH and ΔS separately, both for the ferrites and for the aluminates and gallates.

High-temperature solution calorimetry using a lead borate solvent is a relevant method to determine the enthalpies of solid-state reactions (23–33). The method has been successfully applied to a number of systems. In this study,

TABLE 2
Enthalpy (ΔH_f°) and Entropy (ΔS_f°) of Formation from Monoxides at 298 K for Ferrites Calculated on the Basis of Ref. (21)[a]

Perovskite	ΔH_f° (kJ mol^{-1})	ΔS_f° (J K^{-1} mol^{-1})	Garnet	ΔH_f° (kJ mol^{-1})	ΔS_f° (J K^{-1} mol^{-1})
$LaFeO_3$	-44.35 ± 12.55	24.45 ± 4.18			
$PrFeO_3$	-48.53 ± 12.55	11.90 ± 4.18			
$NdFeO_3$	-44.35 ± 12.55	16.08 ± 4.18			
$SmFeO_3$	-44.35 ± 12.55	11.90 ± 4.18	$Sm_3Fe_5O_{12}$	-238.49 ± 41.84	-24.20 ± 41.84
$EuFeO_3$	-44.35 ± 12.55	7.71 ± 4.18	$Eu_3Fe_5O_{12}$	-238.49 ± 41.84	-28.38 ± 41.84
$GdFeO_3$	-44.35 ± 12.55	7.71 ± 4.18	$Gd_3Fe_5O_{12}$	-234.30 ± 41.84	-28.38 ± 41.84
$TbFeO_3$	-40.17 ± 12.55	7.71 ± 4.18	$Tb_3Fe_5O_{12}$	-209.20 ± 41.84	-15.83 ± 41.84
$DyFeO_3$	-35.98 ± 12.55	7.71 ± 4.18	$Dy_3Fe_5O_{12}$	-184.10 ± 41.84	-3.28 ± 41.84
$HoFeO_3$	-35.98 ± 12.55	3.53 ± 4.18	$Ho_3Fe_5O_{12}$	-133.89 ± 41.84	26.01 ± 41.84
$ErFeO_3$	-35.98 ± 12.55	3.53 ± 4.18	$Er_3Fe_5O_{12}$	-83.68 ± 41.84	55.30 ± 41.84
$TmFeO_3$	-27.61 ± 12.55	7.71 ± 4.18	$Tm_3Fe_5O_{12}$	-58.58 ± 41.84	59.48 ± 41.84
$YbFeO_3$	-23.43 ± 12.55	7.71 ± 4.18	$Yb_3Fe_5O_{12}$	-75.31 ± 41.84	46.93 ± 41.84
$LuFeO_3$	-19.25 ± 12.55	7.71 ± 4.18	$Lu_3Fe_5O_{12}$	-8.37 ± 41.84	80.40 ± 41.84

[a] Perovskites: $\frac{1}{2} Ln_2O_3 + \frac{1}{2} Fe_2O_3 = LnFeO_3$. Garnets: $\frac{3}{2} Ln_2O_3 + \frac{5}{2} Fe_2O_3 = Ln_3Fe_5O_{12}$. ΔH° and ΔS° data of Fe, O_2, and Fe_2O_3 are quoted from Ref. (22). Fe: $\Delta S^\circ = 27.280$ J K^{-1} mol^{-1}, O_2: $\Delta S^\circ = 205.146$ J K^{-1} mol^{-1}, Fe_2O_3: $\Delta H^\circ = -823.411$ kJ mol^{-1}, $\Delta S^\circ = 87.466$ J K^{-1} mol^{-1}.

$Al^{3+}(d^0)$ and $Ga^{3+}(d^{10})$ were chosen as M^{3+}. Enthalpies of solution, ΔH_s, of $LnMO_3$ perovskites (M = Al, Ga), $Ln_3M_5O_{12}$ garnets (M = Al, Ga), α-Al_2O_3, and β-Ga_2O_3 were determined. Using the ΔH_s data and those for Ln_2O_3 measured by Takayama-Muromachi and Navrotsky (34), we will discuss the disproportionation reactions [4] and [6] and the formation reactions [2] and [3] from the viewpoint of the thermodynamic parameters, ΔH, ΔS, and ΔV.

EXPERIMENTAL

Sample Preparation

Ln_2O_3 (Ln = La, Nd, Sm, Eu, Gd, Dy, Ho, Er, Tm, Yb, Lu, Y: 99.9%), α-Al_2O_3 (99.9%), and β-Ga_2O_3 (99.9%) were dried at 1273 K for 1 h, 1273 K for 1 h, and 873 K for 1 h, respectively. They were mixed in stoichiometric ratios for perovskites or garnets using an agate mortar and ethanol. The mixtures for $LnAlO_3$ perovskites (Ln = La, Nd, Sm, Eu, Gd, Dy) were pressed into disks and heated at 1473 K for 1 day in alumina crucibles. The products were ground and examined by powder X-ray diffractometry using Cu$K\alpha$ radiation. Reaction was incomplete so the samples were reground with ethanol, pressed, and heated at 1573 K for 1 day. These grinding and heating procedures were repeated with increasing heating temperature at 100 K intervals until the complete reaction was seen. This step-by-step heating was effective to avoid partial melting. Pure $LnAlO_3$ perovskites (Ln = La, Nd, Sm, Eu, Gd, Dy) were obtained after heating runs at 1773 K. The other samples were prepared similarly with heating runs at 1473, 1573, 1673, and 1973 K for $YAlO_3$ perovskite, 1773 and 1873 K for $Ln_3Al_5O_{12}$ garnets (Ln = Dy, Ho, Er, Tm, Yb, Lu), 1773, 1873, and 1973 K for $Y_3Al_5O_{12}$ garnet, 1473, 1573, and 1673 K twice for $LaGaO_3$ and $NdGaO_3$ perovskites, and one heating run at 1673 K for $Ln_3Ga_5O_{12}$ garnets (Ln = Sm, Eu, Gd, Dy, Ho, Er, Tm, Yb, Lu, Y). Small amounts of Y_2O_3 and α-Al_2O_3 (<5%) were detected in the $YAlO_3$ specimen by powder X-ray diffractometry even after heating at 1973 K. No impurities, such as starting compounds and/or possible coexisting phases, were detected in any other specimen. α-Al_2O_3 and β-Ga_2O_3 were heated respectively at 1773 and 1473 K for 24 h and were ground before calorimetry. Quartz was dried at 573 K before mixture preparation as described next for calorimetry.

TABLE 3
Enthalpy (ΔH_d°) and Entropy (ΔS_d°) of Disproportionation of $LnFeO_3$ and $Ln_3Fe_5O_{12}$ at 298 K for Ferrites Calculated on the Basis of Refs. (21) and (22)[a]

Ln	ΔH_d°[2] (kJ mol^{-1})	ΔS_d°[2] (J K^{-1} mol^{-1})	ΔH_d°[4] (kJ mol^{-1})	ΔS_d°[4] (J K^{-1} mol^{-1})
Sm	-3.3 ± 15.1	-16.7 ± 9.4	105.4 ± 56.3	60.0 ± 43.7
Eu	-3.3 ± 15.1	-13.4 ± 9.4	105.4 ± 56.3	51.5 ± 43.7
Gd	-2.5 ± 15.1	-13.4 ± 9.4	101.3 ± 56.3	51.5 ± 43.7
Tb	-1.7 ± 15.1	-10.9 ± 9.4	88.7 ± 56.3	39.0 ± 43.7
Dy	-0.8 ± 15.1	-8.4 ± 9.4	76.1 ± 56.3	26.4 ± 43.7
Ho	9.2 ± 15.1	1.7 ± 9.4	25.9 ± 56.3	-15.4 ± 43.7
Er	19.2 ± 15.1	7.5 ± 9.4	-24.3 ± 56.3	-44.7 ± 43.7
Tm	15.9 ± 15.1	4.2 ± 9.4	-24.3 ± 56.3	-36.3 ± 43.7
Yb	8.4 ± 15.1	1.7 ± 9.4	5.0 ± 56.3	-23.8 ± 43.7
Lu	17.6 ± 15.1	8.4 ± 9.4	-49.4 ± 56.3	-57.3 ± 43.7

[a] $LnFeO_3 = \frac{1}{5} Ln_3Fe_5O_{12} + \frac{1}{5} Ln_2O_3$: ΔH_d°[2] and ΔS_d°[2]. $Ln_3Fe_5O_{12} = 3\,LnFeO_3 + Fe_2O_3$: ΔH_d°[4] and ΔS_d°[4].

Solution Calorimetry

The high-temperature twin Calvet-type solution calorimeter and the technique used have been described elsewhere

(23, 24). The specimen (8–25 mg) in a platinum sample folder and 30.0 g of $2PbO \cdot B_2O_3$ solvent in a platinum crucible were kept for 8–16 h in the calorimeter at 977 K. The specimen was then dissolved into the molten solvent by several stirrings. After each dissolution run, a reference run with an identical stirring procedure was done to measure the stirring effect. After the experiment, the sample holder was checked by optical microscopy to confirm that all the specimen had been dissolved. Any sample dissolved completely within 45 min as described below. The heats of solution for the specimen were calculated after subtracting the stirring effect. Calibration was achieved by dropping small pieces of platinum into the calorimeters (23).

Rare earth containing oxides are difficult to dissolve in molten lead borate. They react slowly and tend to saturate the melt locally and possibly form borate precipitates (34). Indeed, preliminary experiments showed that none of the binary oxides dissolved completely within 50 min, leading to drawn-out calorimetric cures. The stirring-effect runs also showed large endothermic heat effects, indicating likely slow dissolution during additional stirring. Optical microscopy showed remaining undissolved sample.

To overcome this problem, we prepared a mechanical mixture of the binary oxide and quartz using an agate mortar. As quartz dissolves rapidly, we expected that the rare earth binary oxides would be dispersed in the solvent and precipitate formation would be suppressed. This method was successful. The molar ratios were determined to be $LnMO_3$: $SiO_2 = 1:3$ and $Ln_3M_5O_{12}:SiO_2 = 1:6$ by several trials. All of the mixtures dissolved completely within 40–45 min. Because the heat of solution of SiO_2 (quartz) is small in magnitude (-4.18 ± 0.10 kJ mol^{-1}), the admixture introduced only a small additional heat effect.

To make certain no reaction occurred between the rare earth compound and quartz prior to dissolution, all of the mixtures were kept at 977 K for 24 h and were checked by powder X-ray diffractometry. No reaction was detected. The heats of solution for the binary oxides were calculated by subtracting the heat effect due to quartz from those of the mixtures.

RESULTS

Enthalpies of solution, $\Delta H_s(X)$, in $2PbO \cdot B_2O_3$ at 977 K and enthalpies of formation, $\Delta H_f(X)$, from monoxides at 977 K for binary rare earth oxide phases, X, are given in Table 4. The $\Delta H_s(Ln_2O_3)$ were taken from Ref. (34). $\Delta H_s(LnAlO_3)$ and $\frac{1}{5}\Delta H_s(Ln_3Al_5O_{12}) + \frac{1}{5}\Delta H_s(Ln_2O_3)$ and

TABLE 4
Enthalpy of Solution (ΔH_s) in $2PbO \cdot B_2O_3$ at 977 K for Oxides and Enthalpy of Formation (ΔH_f) from Monoxides at 977 K for Perovskites and Garnets[a]

Compound	ΔH_s (kJ mol^{-1})	ΔH_f (kJ mol^{-1})	Compound	ΔH_s (kJ mol^{-1})	ΔH_f (kJ mol^{-1})
$LaAlO_3$	16.64 ± 1.19 (4)	− 63.17 ± 2.52	$LaGaO_3$	6.08 ± 1.83 (5)	− 50.86 ± 2.92
$NdAlO_3$	15.28 ± 2.88 (7)	− 41.36 ± 3.44	$NdGaO_3$	4.96 ± 2.92 (5)	− 29.29 ± 3.51
$SmAlO_3$	14.32 ± 2.52 (5)	− 37.55 ± 3.26			
$EuAlO_3$	12.79 ± 2.50 (6)	− 30.52 ± 2.60			
$GdAlO_3$	12.50 ± 2.40 (4)	− 32.33 ± 2.96			
$DyAlO_3$	12.41 ± 1.17 (11)	− 21.39 ± 1.35			
$YAlO_3$	9.24 ± 1.72 (7)	− 23.62 ± 1.83			
			$Sm_3Ga_5O_{12}$	118.99 ± 3.86 (6)	− 146.99 ± 7.83
			$Eu_3Ga_5O_{12}$	126.61 ± 3.41 (4)	− 138.11 ± 4.90
			$Gd_3Ga_5O_{12}$	129.26 ± 3.53 (4)	− 147.06 ± 6.86
$Dy_3Al_5O_{12}$	103.66 ± 2.53 (13)	− 97.67 ± 3.43	$Dy_3Ga_5O_{12}$	134.71 ± 3.30 (6)	− 119.96 ± 4.76
$Y_3Al_5O_{12}$	105.23 ± 3.33 (6)	− 115.44 ± 4.00	$Y_3Ga_5O_{12}$	132.10 ± 2.34 (4)	− 133.55 ± 4.09
$Ho_3Al_5O_{12}$	108.50 ± 5.32 (6)	− 101.46 ± 10.05	$Ho_3Ga_5O_{12}$	142.38 ± 3.13 (8)	− 126.58 ± 9.43
$Er_3Al_5O_{12}$	107.60 ± 7.10 (6)	− 96.66 ± 7.69	$Er_3Ga_5O_{12}$	138.68 ± 8.54 (4)	− 118.98 ± 9.38
$Tm_3Al_5O_{12}$	108.89 ± 1.79 (5)	− 97.20 ± 4.80	$Tm_3Ga_5O_{12}$	129.27 ± 6.25 (4)	− 108.82 ± 8.08
$Yb_3Al_5O_{12}$	104.12 ± 3.56 (7)	− 81.03 ± 4.79	$Yb_3Ga_5O_{12}$	126.41 ± 4.41 (5)	− 94.56 ± 6.01
$Lu_3Al_5O_{12}$	103.82 ± 4.78 (10)	− 73.08 ± 5.31	$Lu_3Ga_5O_{12}$	125.53 ± 3.17 (8)	− 86.03 ± 4.67

Compound	ΔH_s (kJ mol^{-1})	Compound	ΔH_s (kJ mol^{-1})	Compound	ΔH_s (kJ mol^{-1})
α-Al_2O_3	32.94 ± 0.59 (9)	B-Sm_2O_3	− 79.4 ± 4.1	C-Ho_2O_3	− 50.2 ± 5.6
β-Ga_2O_3	36.44 ± 1.17 (6)	B-Eu_2O_3	− 68.4 ± 1.3	C-Er_2O_3	− 47.6 ± 1.7
SiO_2(quartz)	− 4.18 ± 0.10 (8)	C-Gd_2O_3	− 72.6 ± 3.4	C-Tm_2O_3	− 47.1 ± 2.8
A-La_2O_3	− 126.0 ± 4.4	C-Dy_2O_3	− 50.9 ± 1.2	C-Yb_2O_3	− 39.5 ± 1.9
A-Nd_2O_3	− 85.1 ± 3.7	C-Y_2O_3	− 61.7 ± 1.1	C-Lu_2O_3	− 34.4 ± 1.2

[a] ΔH_f for perovskites: $\frac{1}{2}Ln_2O_3 + \frac{1}{2}Fe_2O_3 = LnFeO_3$. ΔH_f for garnets: $\frac{3}{2}Ln_2O_3 + \frac{5}{2}Fe_2O_3 = Ln_3Fe_5O_{12}$. The errors are two standard deviations of the mean. The numbers in parentheses are the numbers of experiments. Data for Ln_2O_3 are from Ref. (34).

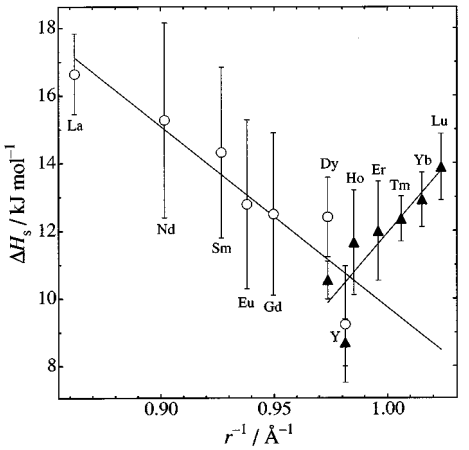

FIG. 1. $\Delta H_s(LnAlO_3)$ (○) and $\frac{1}{5}\Delta H_s(Ln_3Al_5O_{12}) + \frac{1}{5}\Delta H_s(Ln_2O_3)$ (▲) as functions of reciprocal ionic radius of Ln^{3+}, r^{-1}. The $\Delta H_s(Ln_2O_3)$ were taken from Ref. (34).

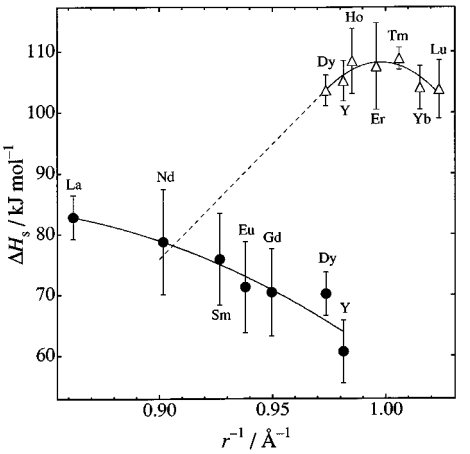

FIG. 3. $3\Delta H_s(LnAlO_3) + \Delta H_s(\alpha\text{-}Al_2O_3)$ (●) and $\Delta H_s(Ln_3Al_5O_{12})$ (△) as functions of r^{-1}.

corresponding data for the Ga system are plotted in Figs. 1 and 2, respectively, as functions of inverse ionic radius (35) of eight-coordinated Ln^{3+}, r^{-1}. The data $\frac{1}{5}\Delta H_s(Ln_3Ga_5O_{12}) + \frac{1}{5}\Delta H_s(Ln_2O_3)$ in Fig. 2 are fitted as a parabolic function of r^{-1}. The other three sets of data in Figs. 1 and 2 are fitted as linear functions of r^{-1}. $\Delta H_s(Ln_3Al_5O_{12})$ and $3\Delta H_s(LnAlO_3) + \Delta H_s(\alpha\text{-}Al_2O_3)$ are plotted against r^{-1} in Fig. 3. They are fitted as parabolic functions of r^{-1} and shown as solid lines in Fig. 3. A dashed line in Fig. 3 is the tangent of $\Delta H_s(Ln_3Al_5O_{12})$ at Ln = Dy. $\Delta H_s(Ln_3Ga_5O_{12})$ and $3\Delta H_s(LnGaO_3) + \Delta H_s(\beta\text{-}Ga_2O_3)$ are plotted against r^{-1} in Fig. 4 and are fitted as parabolic and linear functions of r^{-1}, respectively. A dashed line with positive slope in Fig. 4 is the tangent of $\Delta H_s(Ln_3Ga_5O_{12})$ at Ln = Sm.

DISCUSSION

ΔH and $T\Delta S$ Terms for Reaction [4]

$\Delta H_s(LnAlO_3)$ becomes less positive as r^{-1} increases and becomes negative relative to $\frac{1}{5}\Delta H_s(Ln_3Al_5O_{12}) + \frac{1}{5}\Delta H_s(Ln_2O_3)$ if r^{-1} is larger than that of Dy^{3+} or Y^{3+} (Fig. 1). This means that $LnAlO_3$ perovskites become less stable with increasing r^{-1} at 977 K and that $LnAlO_3$ (Ln = La–Dy, Y) perovskites withstand disproportionation [4] to garnet plus sesquioxide at 977 K, whereas $LnAlO_3$ (Ln = Ho–Lu) perovskites do not. This is consistent with the fact that $LnAlO_3$ (Ln = La–Dy, Y) perovskites can be prepared at ambient pressure (Table 1) whereas high pressure is necessary to obtain $LnAlO_3$ (Ln = Ho–Lu) perovskites (17). The $T\Delta S$ term as well as the ΔH term controls reaction [4] at a given pressure; however, the ΔH term alone is enough to explain the above-mentioned fact. The stability

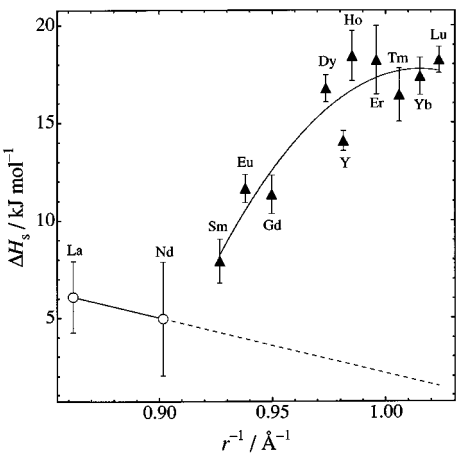

FIG. 2. $\Delta H_s(LnGaO_3)$ (○) and $\frac{1}{5}\Delta H_s(Ln_3Ga_5O_{12}) + \frac{1}{5}\Delta H_s(Ln_2O_3)$ (▲) as functions of r^{-1}.

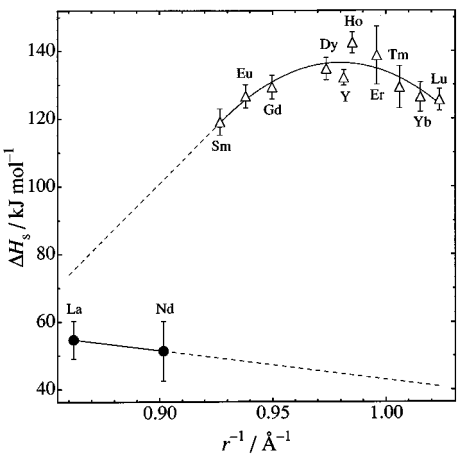

FIG. 4. $3\Delta H_s(LnGaO_3) + \Delta H_s(\beta\text{-}Ga_2O_3)$ (●) and $\Delta H_s(Ln_3Ga_5O_{12})$ (△) as functions of r^{-1}.

of $LnAlO_3$ against reaction [4] is controlled by the ΔH term rather than by the $T\Delta S$ term. The stability of $LnAlO_3$ is controlled by reaction [5] rather than by [4]. The value of $\frac{1}{7}\Delta H_s\,(Ln_3Al_5O_{12}) + \frac{1}{7}\Delta H_s(Ln_4Al_2O_9)$ should be between $\Delta H_s(LnAlO_3)$ and $\frac{1}{5}\Delta H_s(Ln_3Al_5O_{12}) + \frac{1}{5}\Delta H_s(Ln_2O_3)$.

A similar conclusion holds for the stability of $LnGaO_3$ against reaction [4]. $\Delta H_s(LnGaO_3)$ becomes less positive with increasing r^{-1} and is more negative than $\frac{1}{5}\Delta H_s$ $(Ln_3Ga_5O_{12}) + \frac{1}{5}\Delta H_s(Ln_2O_3)$ if r^{-1} is larger than that of Nd^{3+} (Fig. 2). This is consistent with the fact that $LnGaO_3$ (Ln = La–Nd) perovskites can be prepared at ambient pressure (Table 1) whereas high pressure is necessary to obtain $LnGaO_3$ (Ln = Sm–Lu, Y) perovskites (18, 19). Hence, the ΔH term alone is enough to explain the above fact. The stability of $LnGaO_3$ against reaction [4] is controlled by the ΔH term rather than by the $T\Delta S$ term.

ΔS should be determined experimentally to confirm the foregoing discussion quantitatively. ΔS can be determined, for example, by measuring specific heats of the perovskites, garnets, Ln_2O_3 phases, and M_2O_3 phases. Corresponding data for Ln_2O_3 and M_2O_3 phases are compiled in Ref. 22. At least, the present work indicates qualitatively that the stability of the perovskites against reaction [4] is controlled by the ΔH term rather than by the $T\Delta S$ term.

*P*Δ*V* Terms for Reaction [4]

Ln_2O_3 phases crystallize in A-type (Ln = La–Nd), B-type (Ln = Sm, Eu), and C-type (Ln = Gd–Lu, Y) structures at ambient pressure. The molar volume of Ln_2O_3 increases upon transitions from A to B type and from B to C type (Table 5). Therefore, Ln_2O_3 has a tendency to transform from C to B type and from B to A type under pressure. C-Ln_2O_3 (Ln = Gd–Lu, Y) phases transform to B type at 2.5–4.0 MPa and at 1178–1293 K. B-Ln_2O_3 (Ln = Gd–Lu, Y) phases are quenchable to ambient pressure and room temperature (36). B-Sm_2O_3 transforms to A type at 3 GPa and at room temperature, but A-Sm_2O_3 reverts to B type when pressure is released (37).

Here we discuss the $P\Delta V$ terms for reaction [4]. ΔH and ΔV values for reaction [4] are shown in Table 6. ΔH data at 977 K are obtained from the fitted lines in Figs. 1 and 2. ΔV values are derived from the values shown in Table 5 and are assumed to be independent of pressure. Figures 5 and 6 show the pressure dependence of ΔG at 977 K for the reactions $LnAlO_3 = \frac{1}{5}Ln_3Al_5O_{12} + \frac{1}{5}Ln_2O_3$ and $LnGaO_3 = \frac{1}{5}Ln_3Ga_5O_{12} + \frac{1}{5}Ln_2O_3$, respectively. The enthalpies of transitions among A-, B-, and C-Ln_2O_3 are expected to be small (34), for example, about 3 kJ mol^{-1} for B to C in Sm_2O_3 (22). The magnitude, 3 kJ mol^{-1}, does not seem to seriously affect the energetics of reaction [4]. Without detailed study for other systems, the enthalpies of transitions are neglected in this discussion. Figure 5 indicates that all of the $LnAlO_3$ perovskites (Ln = Ho–Lu), which cannot be synthesized by conventional solid-state reactions at ambient pressure, are stable against reaction [4] at 977 K if a pressure of 1.3–1.4 GPa or higher is applied. Ln_2O_3 oxides (Ln = Dy–Lu, Y) below 1.4 GPa and at 977 K should be C type (36). This is consistent with the result of Dernier *et al.* (17). They synthesized $LnAlO_3$ perovskites (Ln = Ho–Lu) at 3.25 GPa and 1473 ± 10 K (17). Figure 6 shows that all of the $LnGaO_3$ perovskites (Ln = Sm–Lu, Y), which cannot be obtained by solid-state reactions at ambient pressure, are stable against reaction [4] at 977 K if a pressure of about 4.6–5.6 GPa or higher is applied. Specifically, about 1 GPa is enough to prevent reaction [4] at 977 K for $SmGaO_3$. Sm_2O_3 at around 1 GPa and at 977 K maintains the B form (37). Ln_2O_3 (Ln = Eu–Lu, Y) phases at around 5–6 GPa and at 977 K crystallize in B or C type (36), This is consistent with the result of Marezio *et al.* (18, 19). They synthesized $LnGaO_3$ perovskites (Ln = Sm–Lu, Y) at 7 GPa

TABLE 5
Volume per Unit Formula (Å^3 (unit formula)$^{-1}$) for Oxides[a]

Ln	A-Ln_2O_3	B-Ln_2O_3	C-Ln_2O_3	$LnAlO_3$	$Ln_3Al_5O_{12}$	$LnGaO_3$	$Ln_3Ga_5O_{12}$
La	82.3002[45]		90.8290[48]	54.4655[60]		58.7259[19]	
Nd	76.2074[45]		85.0157[49]	52.8028[61]		57.5649[19]	244.4924[67]
Sm		74.7996[46]	81.5423[50]	52.3041[61]		56.6805[19]	240.1779[68]
Eu		73.4338[45]	80.2352[51]	51.9958[17]		56.4097[19]	238.3857[69]
Gd		72.0722[47]	79.0167[52]	51.8227[17]	222.1596[39]	56.0332[19]	237.3434[70]
Dy		69.8850[45]	75.8163[53]	51.1690[17]	217.7869[63]	55.2166[19]	233.0057[71]
Y		68.3005[45]	74.5228[54]	50.8510[62]	216.0000[39]	54.8078[18]	231.4755[39]
Ho		68.4558[45]	74.6536[55]	50.8416[17]	216.0000[64]	54.7175[19]	231.5321[72]
Er		67.5456[45]	73.3484[56]	50.5308[17]	213.9545[65]	54.4517[19]	230.0647[73]
Tm		66.4109[45]	72.1038[57]	50.2400[17]	213.6863[66]	54.0554[19]	228.5474[74]
Yb		65.2021[45]	71.0366[58]	49.9622[17]	212.2954[39]	53.7334[19]	227.2043[39]
Lu		64.5577[45]	70.1014[59]	49.6365[17]	210.9637[39]	53.4356[19]	226.3119[39]
	α-Al_2O_3	42.4207[75]	α-Ga_2O_3	48.1335[76]	β-Ga_2O_3	52.3761[77]	

[a] Superscripts show reference numbers.

TABLE 6
ΔH^a at 977 K, ΔS^b, and ΔV of Disproportionation of Perovskites and Garnets[c]

Perovskite	ΔH (kJ mol^{-1})	ΔV(A) (cm^3 mol^{-1})	ΔV(B) (cm^3 mol^{-1})	ΔV(C) (cm^3 mol^{-1})
$DyAlO_3$	− 1.271		3.8333	4.5477
$YAlO_3$	− 0.264		3.6187	4.3682
$HoAlO_3$	0.245		3.6429	4.3894
$ErAlO_3$	1.667		3.4742	4.1730
$TmAlO_3$	2.987		3.4804	4.1661
$YbAlO_3$	4.198		3.3347	4.0375
$LuAlO_3$	5.293		3.2932	3.9608
$NdGaO_3$	− 2.870	3.9594		5.0204
$SmGaO_3$	4.016		3.8027	4.6148
$EuGaO_3$	6.619		3.5856	4.4047
$GdGaO_3$	8.962		3.5230	4.3594
$DyGaO_3$	12.780		3.2286	3.9429
$YGaO_3$	13.698		3.0997	3.8492
$HoGaO_3$	14.108		3.1795	3.9260
$ErGaO_3$	15.060		3.0533	3.7522
$TmGaO_3$	15.688		2.9729	3.6586
$YbGaO_3$	16.049		2.8594	3.5622
$LuGaO_3$	16.198		2.8533	3.5209

Garnet	ΔH (kJ mol^{-1})	ΔS (J K^{-1} mol^{-1})	$\Delta V(\alpha)$ (cm^3 mol^{-1})	$\Delta V(\beta)$ (cm^3 mol^{-1})
$La_3Al_5O_{12}$	− 21.226	14.21		
$Nd_3Al_5O_{12}$	− 2.198	14.21		
$Sm_3Al_5O_{12}$	10.978	14.21		
$Eu_3Al_5O_{12}$	17.208	14.21		
$Gd_3Al_5O_{12}$	23.779	14.21	− 14.6157	
$Dy_3Al_5O_{12}$	38.383	14.21	− 13.1638	
$Y_3Al_5O_{12}$	42.623	14.21	− 12.6621	
$Ho_3Al_5O_{12}$	44.450	14.21	− 12.6784	
$Er_3Al_5O_{12}$	48.417	14.21	− 12.0081	
$Tm_3Al_5O_{12}$	50.608	14.21	− 12.3725	
$Yb_3Al_5O_{12}$	51.355	14.21	− 12.0370	
$Lu_3Al_5O_{12}$	50.990	14.21	− 11.8245	
$La_3Ga_5O_{12}$				
$Nd_3Ga_5O_{12}$	50.655		− 14.2508	− 11.6956
$Sm_3Ga_5O_{12}$	69.636		− 13.2499	− 10.6947
$Eu_3Ga_5O_{12}$	77.378		− 12.6603	− 10.1051
$Gd_3Ga_5O_{12}$	83.626		− 12.7133	− 10.1581
$Dy_3Ga_5O_{12}$	91.155		− 11.5758	− 9.0206
$Y_3Ga_5O_{12}$	92.009		− 11.3933	− 8.8381
$Ho_3Ga_5O_{12}$	92.158		− 11.5896	− 9.0344
$Er_3Ga_5O_{12}$	91.569		− 11.1867	− 8.6315
$Tm_3Ga_5O_{12}$	89.697		− 10.9898	− 8.4346
$Yb_3Ga_5O_{12}$	86.857		− 10.7628	− 8.2076
$Lu_3Ga_5O_{12}$	83.364		− 10.7622	− 8.2070

[a] Derived from the fitting lines shown in Figs. 1–4.
[b] See text.
[c] Perovskites: $LnMO_3 = \frac{1}{5} Ln_3M_5O_{12} + \frac{1}{5}$(A-, B-, or C-) Ln_2O_3. Garnets: $Ln_3M_5O_{12} = 3\,LnMO_3 + (\alpha$- or β-$)M_2O_3$.

and 1273 K or at 4.5 GPa and 1273 K. The disproportionation reaction [4] is controlled almost by the ΔH and $P\Delta V$ terms. Contribution of the $T\Delta S$ term to reaction [4] is small.

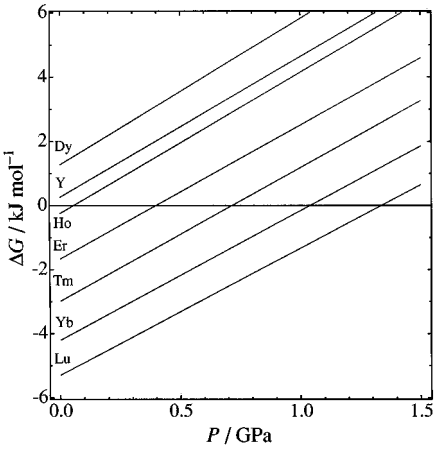

FIG. 5. ΔG versus pressure at 977 K for the reaction $LnAlO_3 = \frac{1}{5} Ln_3Al_5O_{12} + \frac{1}{5}$C-$Ln_2O_3$.

ΔH *and* $T\Delta S$ *Terms for Reaction* [6]

If we try to prepare $Ln_3Al_5O_{12}$ from a stoichiometric mixture of monoxides by conventional methods at ambient pressure, the product is $Ln_3Al_5O_{12}$ garnet for Ln = Dy–Lu and Y and is a $3\,LnAlO_3 + \alpha$-Al_2O_3 mixture for the others (Table 1). The enthalpy data shown in Fig. 5 are, at a glance, in conflict with the data given in Table 1. Figure 5 indicates that not only $Ln_3Al_5O_{12}$ (Ln = Dy–Lu, Y) but also $Eu_3Al_5O_{12}$ and $Gd_3Al_5O_{12}$ garnets are stable against the disproportionation reaction [6] at 977 K. The entropy term explains why $Ln_3Al_5O_{12}$ (Ln = Eu, Gd) cannot be prepared by conventional solid-state reaction. The garnets (Ln = Dy–Lu, Y) are stable at 1873 K. Indeed, our garnet specimens (Ln = Dy–Lu) are prepared at 1873 K and the $Y_3Al_5O_{12}$ one at 1973 K. On the other hand, $Gd_3Al_5O_{12}$ was synthesized by heating a stoichiometric, amorphous

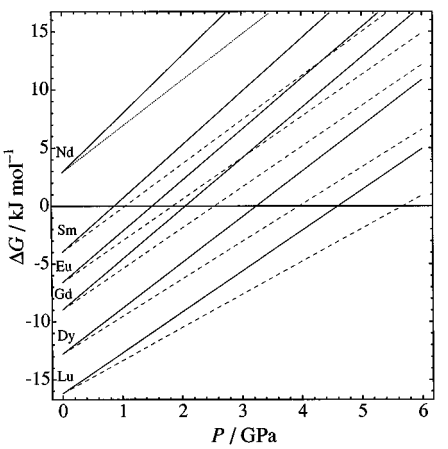

FIG. 6. ΔG versus pressure at 977 K for the reactions $NdGaO_3 = \frac{1}{5} Nd_3Ga_5O_{12} + \frac{1}{5}$A-$Nd_2O_3$ (dotted line), $LnGaO_3 = \frac{1}{5} Ln_3Ga_5O_{12} + \frac{1}{5}$B-$Ln_2O_3$ (dashed lines), and $LnGaO_3 = \frac{1}{5} Ln_3Ga_5O_{12} + \frac{1}{5}$C-$Ln_2O_3$ (solid lines).

sample at 1573 K for 1 h in air followed by rapid quenching (15). $Gd_3Al_5O_{12}$ decomposed into $3GdAlO_3 + \alpha$-Al_2O_3 after being maintained at 1773 K for 24 h in air. $Gd_3Al_5O_{12}$ is a low-temperature state and the mixture $3GdAlO_3 + \alpha$-Al_2O_3 is a high-temperature state. The difference between $\Delta H_s(Ln_3Al_5O_{12})$ and $3\Delta H_s(LnAlO_3) + \Delta H_s(\alpha\text{-}Al_2O_3)$ in Fig. 3 is attributable to the $T\Delta S$ term. The stability of $Ln_3Al_5O_{12}$ against reaction [6] is controlled by the $T\Delta S$ term as well as by the ΔH term.

According to Shishido *et al.* (15), ΔG for reaction [6] with Ln = Gd and M = Al is zero at a temperature between 1573 and 1773 K. Here we assume that ΔG is zero at 1673 K. ΔH for reaction [6] with Ln = Gd and M = Al is estimated to be 23.78 kJ mol^{-1} by extrapolation lines shown in Fig. 3. Consequently, $\Delta S^{1673\,K}$ for reaction [6] with Ln = Gd and M = Al is 14.21 J K^{-1} mol^{-1}. If we further assume that the ΔS term is independent of both temperature and Ln element, we can calculate the ΔG values as functions of temperature (Fig. 7). The equilibrium temperatures, T_{eq}, for Eq. [6] are calculated to be 3000 (Ln = Y), 2701 (Ln = Dy), 1673 (Ln = Gd), 1211 (Ln = Eu), 773 (Ln = Sm), and −155 K (Ln = Nd). It is, thus, predicted that $Eu_3Al_5O_{12}$ and $Sm_3Al_5O_{12}$ can be obtained if synthetic temperatures are decreased, as in the case with $Gd_3Al_5O_{12}$.

The corresponding Ga system shows a similar tendency. If we try to prepare $Ln_3Ga_5O_{12}$ from a stoichiometric mixture of monoxides at ambient pressure, the product is $Ln_3Ga_5O_{12}$ garnet for Ln = Nd–Lu and Y and is $3\,LnGaO_3 + \beta$-Ga_2O_3 for the others (Table 1). The corresponding synthesis for $LnGaO_3$ results in $\frac{1}{7}Ln_3M_5O_{12} + \frac{1}{7}Ln_4M_2O_9$ (Ln = Sm–Gd) (10) or $\frac{1}{5}Ln_3M_5O_{12} + \frac{1}{5}Ln_2O_3$ (Ln = Tb–Lu). On the other hand, Geller *et al.* (16) prepared $LnGaO_3$ perovskites (Ln = Sm–Er) by quenching molten mixtures of Ln_2O_3 and Ga_2O_3. The molten state was kept at approximately 1923 K for $SmGaO_3$ and approximately 2273 K for $ErGaO_3$ for about 10 min and then quenched. The $LnGaO_3$ perovskites were obtained as a single phase except for $HoGaO_3$ and $ErGaO_3$. These results suggest that $Ln_3Ga_5O_{12}$ garnets are the lower temperature states and the corresponding mixtures, $3\,LnGaO_3 + \beta$-Ga_2O_3, are the higher temperature states. Indeed, there also is a difference between $\Delta H_s(Ln_3Ga_5O_{12})$ and $3\,\Delta H_s(LnGaO_3) + \Delta H_s(\beta\text{-}Ga_2O_3)$ in Fig. 4. Figure 4 predicts that $Ln_3Ga_5O_{12}$ garnets with Ln = La–Pr would also be stable against reaction [6] at 977 K or below. The stability of $Ln_3Ga_5O_{12}$ against reaction [6] is controlled by the $T\Delta S$ term as well as by the ΔH term.

*P*Δ*V* Terms for Reaction [6]

Here we discuss the $P\Delta V$ terms for reaction [6]. ΔH, ΔS, and ΔV values for reaction [4] are shown in Table 6. ΔH data at 977 K are obtained from the fitted lines in Figs. 3 and 4. ΔS values are estimated by the above discussion. ΔV values are derived from the values shown in Table 5 and are assumed to be independent of pressure. Figures 8 and 9 show the pressure dependence of ΔG at 977 K for the reactions $Ln_3Al_5O_{12} = 3\,LnAlO_3 + Al_2O_3$ and $Ln_3Ga_5O_{12} = 3\,LnGaO_3 + Ga_2O_3$, respectively. Ambient-pressure phase β-Ga_2O_3 transforms to corundum-type α-Ga_2O_3 at 4.4 GPa and 1273 K (38). The enthalpy of transition between α- and β-Ga_2O_3 phases should be studied to analyze the $P\Delta V$ terms for reaction [6]. However, the enthalpy of transition is neglected in this discussion in analogy to the enthalpy of transition among A-, B-, and C-Ln_2O_3. Figures 8 and 9 indicate that, even if the $T\Delta S$ term is disregarded, none of the $Ln_3M_5O_{12}$ phases is thermodynamically stable against the disproportionation [6] at pressures of about 4.3 GPa or higher (M = Al) or about 8.2 GPa or higher (M = Ga), respectively.

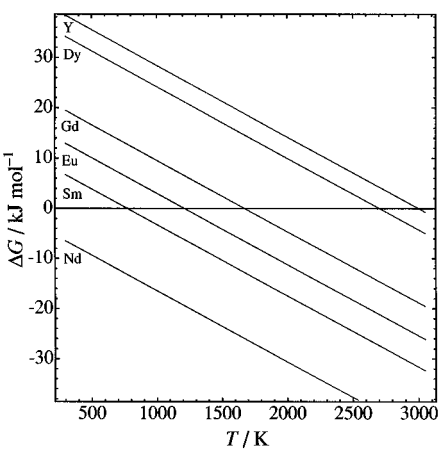

FIG. 7. ΔG versus temperature for the reaction $Ln_3Al_5O_{12} = 3LnAlO_3 + \alpha$-$Al_2O_3$.

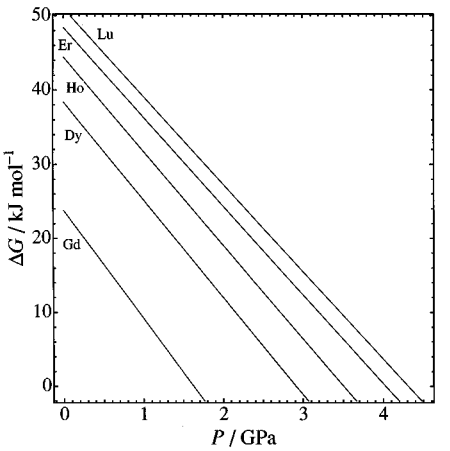

FIG. 8. ΔG versus pressure at 977 K for the reaction $Ln_3Al_5O_{12} = 3\,LnAlO_3 + \alpha$-$Al_2O_3$.

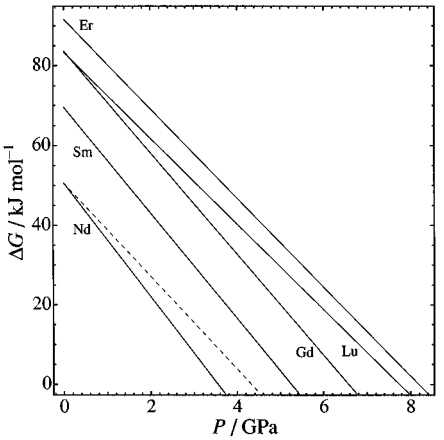

FIG. 9. ΔG versus pressure at 977 K for the reactions $Ln_3Ga_5O_{12} = 3\,LnGaO_3 + \alpha\text{-}Ga_2O_3$ (solid lines) and $Nd_3Ga_5O_{12} = 3\,NdGaO_3 + \beta\text{-}Ga_2O_3$ (dashed line).

Factors Controlling the ΔH_s of Perovskites and Garnets

In both $LnMO_3$ perovskites and $Ln_3M_5O_{12}$ garnets, *Ln*–O distances change depending on *Ln* but *M*–O distances are almost independent of *Ln* (14, 39). In $LnMO_3$ perovskites, the twelve *Ln*–O distances can be approximately classified into two types, eight shorter and four longer. The twelve O and *Ln* atoms form face centered cubic type close-packed layers, if distortion is disregarded. The eight O atoms with shorter bond lengths coordinate to the *Ln* atom in a distorted bicapped trigonal prism. Energetic terms might scale with a potential term, r^{-1}, but bond lengths vary directly with ionic radius. The difference between the mean *Ln*–O distance of the shorter eight and that of the longer four increases with increasing r^{-1} (Table 7, Fig. 10) (14). Consequently, the distortion of the *Ln* coordination polyhedra increases markedly with increasing r^{-1} (14). In $Ln_3M_5O_{12}$ garnets, *Ln* atoms are coordinated by eight O atoms in a distorted CsCl-type coordination (Fig. 11). The eight *Ln*–O distances consist of two types, four shorter and four longer, though the eight O atoms are crystallographically equivalent. Both types of *Ln*–O distances decrease with increasing r^{-1} (Table 7, Fig. 10) (39). Therefore, the distortion of the *Ln* coordination polyhedra in the garnets does not change as a function of r^{-1}, but the corresponding distortion in the perovskites does.

$\Delta H_s(LnMO_3)$ decreases linearly with increasing r^{-1} in both the Al and Ga systems (Figs. 1 and 2). The $\Delta H_s(Ln_3M_5O_{12})$ versus r^{-1} curves are concave upward and show positive peaks at around Ln = Er for the Al system and at around Ln = Y for the Ga system (Figs. 3 and 4). The slope for $\Delta H_s(LnMO_3)$ versus r^{-1} is larger than both positive and negative slopes for $\Delta H_s(Ln_3M_5O_{12})$ versus r^{-1}, if the slopes are normalized per mole of oxygen atom. These features reflect the extent of the distortion of the *Ln* coordination polyhedra. The distortion is large in perovskites and small in garnets. The positive peaks of $\Delta H_s(Ln_3M_5O_{12})$ indicate that there is an optimum ionic radius of Ln^{3+} for Al and Ga garnets. The eight O atoms surrounding a Ln^{3+} form a distorted cube. Among the twelve edges of the cube, four are shared by another *Ln*O polyhedron, four by *M*O octahedra, and two by *M*O tetrahedra. The location of the three types of shared edges shows a C_2 rotation axis (Fig. 11). There should be strong interaction among the lengths of the three types of edges. Consequently, there should be an optimum size of Ln^{3+} to share the edges with *M*O octahedra, *M*O tetrahedra, and *Ln*O polyhedra. This probably causes the positive peaks of $\Delta H_s(Ln_3M_5O_{12})$. Indeed, Al^{3+} is smaller than Ga^{3+}, and the optimum Ln^{3+} is smaller for Al garnet (Er^{3+}) and larger for Ga garnet (Y^{3+}) (Figs. 3 and 4). A similar discussion has been applied to the Fe garnets by Kimizuka *et al.* (21). Their calculation of Madelung energies indicated that Tb^{3+} has the optimum radius in the Fe

TABLE 7
Mean *Ln*–O Distances (Å) in Perovskites and Garnets[a]

Ln	*Ln*–O_{12}	*Ln*–O_{8short}	*Ln*–O_{4long}	*Ln*–O_{short}	*Ln*–O_{long}
	LnAlO_3			*Ln*$_3Al_5O_{12}$	
Nd	2.660[61]	2.5915[61]	2.797[61]		
Sm	2.6575[61]	2.4995[61]	2.9735[61]		
Gd				2.335[39]	2.458[39]
Y	2.6552[82]	2.4011[82]	3.1633[82]	2.303[39]	2.432[39]
Er				2.298[65]	2.428[65]
Yb				2.283[39]	2.397[39]
Lu				2.276[39]	2.383[39]
	LnGaO_3			*Ln*$_3Ga_5O_{12}$	
Gd	2.7564[83]	2.4646[83]	3.340[83]	2.359[70]	2.473[70]
Tb				2.364[81]	2.455[81]
Y				2.338[39]	2.428[39]
Yb				2.302[39]	2.407[39]
Lu				2.303[39]	2.393[39]
	LnFeO_3			*Ln*$_3Fe_5O_{12}$	
La	2.7982[84]	2.6049[84]	3.1848[84]		
Pr	2.7899[14]	2.5446[14]	3.2805[14]		
Nd	2.7898[14]	2.5266[14]	3.3160[14]		
Sm	2.7853[14]	2.4929[14]	3.3700[14]	2.394[39]	2.489[39]
Eu	2.7833[14]	2.4788[14]	3.3925[14]		
Gd	2.7820[14]	2.4675[14]	3.4110[14]	2.38[78]	2.47[78]
Tb	2.7756[14]	2.4535[14]	3.4198[14]	2.368[79]	2.462[79]
Dy	2.7727[14]	2.4415[14]	3.4350[14]	2.360[39]	2.439[39]
Y	2.7710[85]	2.4308[85]	3.4515[85]	2.357[80]	2.436[80]
Ho	2.7681[14]	2.4306[14]	3.4430[14]		
Er	2.7657[14]	2.4210[14]	3.4550[14]		
Tm	2.7636[14]	2.4140[14]	3.4628[14]		
Yb	2.7587[14]	2.4023[14]	3.4715[14]	2.335[39]	2.417[39]
Lu	2.7548[14]	2.3953[14]	3.4738[14]	2.319[39]	2.385[39]
Lu				2.326[39]	2.385[39]

[a] Superscripts show reference numbers.

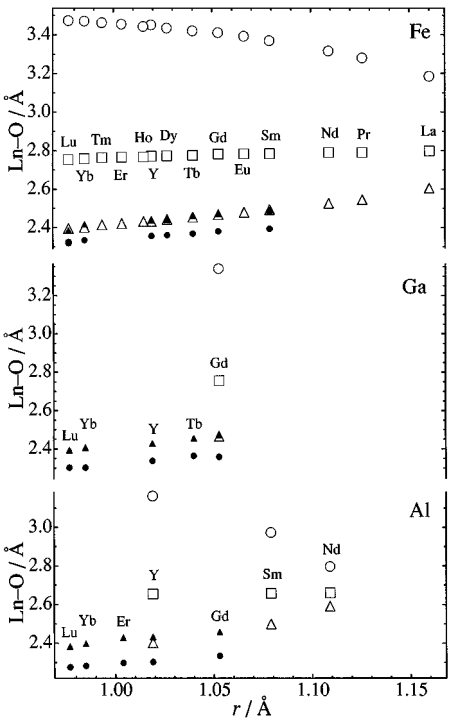

FIG. 10. Mean *Ln*–O distances as functions of *r*. Closed circles and closed triangles indicate the shorter *Ln*–O and the longer *Ln*–O distances in garnets, respectively. Open circles, open triangles, and open squares show the mean *Ln*–O distance of the longer four *Ln*–O distances, the mean *Ln*–O distance of the shorter eight *Ln*–O distances, and the mean *Ln*–O distance of the twelve *Ln*–O distances in perovskites, respectively. Upper, middle, and lower figures represent Fe, Ga, and Al systems, respectively.

garnets (21). Fe^{3+} and Tb^{3+} are larger than Ga^{3+} and Y^{3+}, respectively (35). From this point of view, the calculation of Kimizuka *et al.* and our results are consistent. The ΔH_s of the perovskites and the garnets is controlled mainly by the distortion of the *Ln*O polyhedra.

Factors Controlling the ΔS of Reaction [6]

Reaction [6] shows positive ΔS and negative ΔV; therefore, the boundary between $Ln_3M_5O_{12}$ and $3LnMO_3 + M_2O_3$ has a negative slope in the *P*–*T* diagram (Fig. 12). *Ln* cations are eight-coordinated, two-fifths of *M* cations are six-coordinated, and the other *M* ions are four-coordinated in $Ln_3M_5O_{12}$. In $LnMO_3$, the *Ln* cations are between twelve- and eight-coordinated, depending on the distortion, and the *M* cations are six-coordinated. The *M* cations in α-M_2O_3 are six-coordinated. In β-Ga_2O_3, half the Ga cations are six-coordinated and the other half, four coordinated. Consequently, the mean coordination numbers of both Ln^{3+} and M^{3+} increase by the disproportionation reaction [6]. The reaction also elongates both the mean *Ln*–O distance and the mean *M*–O distance. The mean *Ln*–O distance of the shorter eight *Ln*–O bonds in $LnMO_3$ is almost equal to the longer *Ln*–O distance in $Ln_3M_5O_{12}$ and is shorter than the shorter *Ln*–O distance in $Ln_3M_5O_{12}$ (Fig. 10). Therefore, the mean *Ln*–O distance increases in reaction [6] even if the coordination number of Ln^{3+} in $LnMO_3$ is regarded as eight. Both the increase in coordination number and elongation in bond distance result in a positive ΔS (40, 41). The perovskite-forming reactions have a negative ΔV, despite an increase in local coordination number and bond length. More efficient overall packing decreases the volume. Though the decrease in volume would tend to decrease the entropy, the weaker *Ln*–O bonds result in an increase in entropy which more than compensates, and the overall ΔS of perovskite-forming reactions are generally positive (40) as has been seen for $CdTiO_3$ and $CdSnO_3$ perovskites (42) and for $MgSiO_3$ perovskite (43). An analogous tendency has been reported for molten states of aluminosilicates (44). The viscosity of aluminosilicate melts decreases with increasing pressure, which is accompanied by both an increasing coordination number of

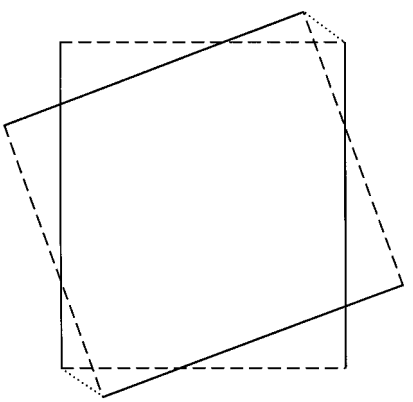

FIG. 11. Schematic illustration of the distorted CsCl-type coordination of Ln^{3+} in garnets. O atoms are located at the corners and the Ln^{3+} in the center of the distorted cube. Solid, dashed, and dotted lines indicate the shared edges with another *Ln*O coordination polyhedron, *M*O octahedra, and *M*O tetrahedra, respectively.

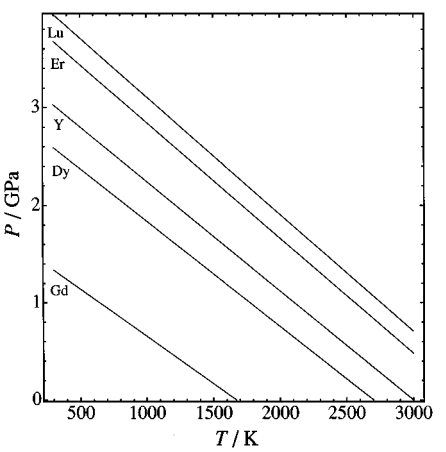

FIG. 12. *P*–*T* boundaries between $Ln_3Al_5O_{12}$ (lower left) and $3\,LnAlO_3 + \alpha$-Al_2O_3 (upper right).

Al and a weakening of the Al–O bond strength. Negative ΔV values for reaction [6] are achieved by not only an increase in coordination number but also an *increase* in bond distance. This causes the negative slope in the P–T diagram.

Formation Reactions [2] and [3]

Enthalpies of formation (ΔH_f) of perovskites and garnets from monoxides are shown as functions of r^{-1} in Fig. 13 for the Al system and in Fig. 14 for the Ga system, respectively. ΔH_f values of both Al and Ga perovskites become more negative with increasing r^{-1}. This tendency reflects both the negative slope for $\Delta H_s(LnMO_3)$ versus r^{-1} and the positive slope for $\Delta H_s(Ln_2O_3)$ versus r^{-1}. The negative slope for the former was discussed earlier. The positive slope for the latter is caused by the strengthening of the ionic bond by shortening of the Ln–O distance from Ln = La to Ln = Lu. Corresponding strengthening occurs in the shorter eight Ln–O bonds in $LnMO_3$. However, the strengthening is overcome by the weakening of the ionic bond between Ln and the distant four O atoms. The distances between Ln and the more distant four O atoms increase with increasing r^{-1}, as described earlier.

The f orbitals in La^{3+} and Y^{3+} are vacant and those of Gd^{3+} are half-filled; therefore, the three Ln^{3+} are free from any crystal field stabilization but the other Ln^{3+} are not. The dashed line in Fig. 13 is fitted for the three $LnAlO_3$ (Ln = La, Gd, Y). The positive deviation from the line for the remaining $LnAlO_3$ perovskites may reflect the crystal field stabilization of Ln^{3+} in Ln_2O_3 (34).

ΔH_f values of $Ln_3Al_5O_{12}$ (Ln = Dy–Er, Y) and $Ln_3Ga_5O_{12}$ (Ln = Sm–Gd) are almost constant and become less negative with decreasing ionic radius of Ln^{3+} (Figs. 13 and 14). This tendency reflects both the positive peaks in

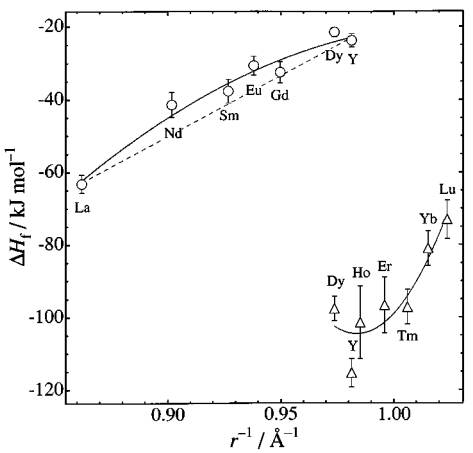

FIG. 13. $\Delta H_f(LnAlO_3)$ (○) and $\Delta H_f(Ln_3Al_5O_{12})$ (△) as functions of r^{-1}. The dashed line is fitted for the three $\Delta H_f(LnAlO_3)$ values with Ln = La, Gd, and Y.

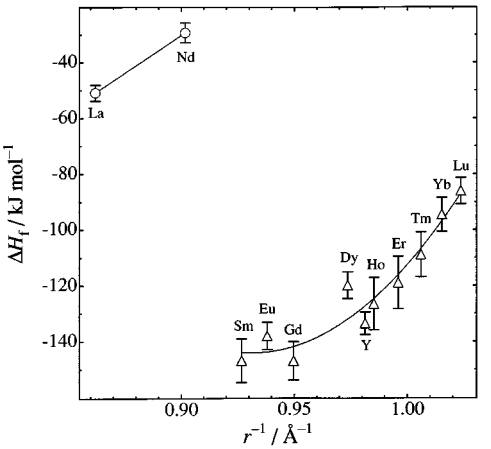

FIG. 14. $\Delta H_f(LnGaO_3)$ (○) and $\Delta H_f(Ln_3Ga_5O_{12})$ (△) as functions of r^{-1}.

$\Delta H_s(Ln_3M_5O_{12})$ versus r^{-1} and the positive slope for $\Delta H_s(Ln_2O_3)$ versus r^{-1}, as already discussed. $\Delta H_s(Ln_3M_5O_{12})$ versus r^{-1} curves are concave downward, slightly, in both Al and Ga systems. This suggests that the formation reaction [3] is influenced by the deviation of the ionic radius of Ln^{3+} from the optimum size for the garnet structure rather than the crystal field stabilization of Ln^{3+} in Ln_2O_3.

Finally, we discuss the ΔS of the formation reactions [2] and [3]. In both Al and Ga systems, the following two relations hold:

$$Ln_3M_5O_{12} = 3\,LnMO_3 + M_2O_3 \qquad \Delta S > 0 \qquad [9]$$

$$LnMO_3 = \tfrac{1}{5}Ln_3M_5O_{12} + \tfrac{1}{5}Ln_2O_3 \qquad \Delta S \approx 0. \qquad [10]$$

Negative entropies of formation of both the perovskites and the garnets are deduced from [9] and [10] as follows:

$$\tfrac{1}{2}Ln_2O_3 + \tfrac{1}{2}M_2O_3 = LnMO_3 \qquad \Delta S < 0 \qquad [11]$$

$$\tfrac{3}{2}Ln_2O_3 + \tfrac{5}{2}M_2O_3 = Ln_3M_5O_{12} \qquad \Delta S < 0. \qquad [12]$$

On the basis of the "ΔH and $T\Delta S$ terms for reaction [6]" section, ΔS values for [9] in the Al system are assumed to be 14.21 J K^{-1} mol^{-1}. Provided that ΔS values for [10] in the Al system are zero, the following two relationships hold:

$$\tfrac{1}{2}Ln_2O_3 + \tfrac{1}{2}\alpha\text{-}Al_2O_3 = LnAlO_3$$

$$\Delta S = -7.11\ \mathrm{J\,K^{-1}\,mol^{-1}} \qquad [13]$$

$$\tfrac{3}{2}Ln_2O_3 + \tfrac{5}{2}\alpha\text{-}Al_2O_3 = Ln_3Al_5O_{12}$$

$$\Delta S = -35.53\ \mathrm{J\,K^{-1}\,mol^{-1}}. \qquad [14]$$

These negative ΔS values suggest that Ln_2O_3 phases possess relatively large entropies.

CONCLUSION

High-temperature solution calorimetry using a $2PbO \cdot B_2O_3$ solvent at 977 K was performed for $LnMO_3$ perovskites and $Ln_3M_5O_{12}$ garnets (Ln = La–Lu, Y; M = Al, Ga), α-Al_2O_3, and β-Ga_2O_3. The stability of $LnMO_3$ against the disproportionation to garnet plus sesquioxide is controlled almost entirely by ΔH and $P\Delta V$ but not by $T\Delta S$. On the contrary, the stability of $Ln_3Al_5O_{12}$ against disproportionation to perovskites plus sesquioxide is controlled not only by ΔH and $P\Delta V$ but also by $T\Delta S$. The P–T boundary between $Ln_3M_5O_{12}$ and $3LnMO_3 + M_2O_3$ has a negative slope. The positive ΔS and negative ΔV for the disproportionation are caused by an increase in coordination number and an *increase* in bond distance. ΔH for perovskite formation is mainly controlled by two factors, the strengthening of the ionic bond in Ln_2O_3 with decreasing ionic radius of Ln^{3+}, and the *weakening* of the ionic bond between Ln and the distant four O atoms in $LnMO_3$ with decreasing ionic radius of Ln^{3+}. ΔH of garnet formation is mainly controlled by two factors, the strengthening of the ionic bond in Ln_2O_3 with decreasing ionic radius of Ln^{3+}, and the deviation of the ionic radius of Ln^{3+} from the optimum size for the garnet structure. ΔS values of both perovskite formation and garnet formation are deduced to be negative, which suggests that Ln_2O_3 phases possess relatively large entropies.

ACKNOWLEDGMENTS

This study was supported by the STA fellowship provided by the Science and Technology Agency, Japan, and by the National Science Foundation (Grant DMR 92-15802). Valuable discussions with Drs. L. Topor and E. Takayama-Muromachi are much appreciated. We thank Drs. K. Bose and I. Petrovic for helpful suggestions on the calorimetry experiments.

REFERENCES

1. G. A. Massey and J. M. Yarborough, *Appl. Phys. Lett*. **18,** 576 (1971).
2. B. Struve, G. Huber, V. V. Laptev, I. A. Shcherbakov, and E. V. Zharikov, *Appl. Phys. B*: *Photophys. Laser Chem.* **30,** 117 (1983).
3. J. E. Greedan, *J. Less-Common Met*. **111,** 335 (1985).
4. P. Dougier and P. Hagenmuller, *J. Solid State Chem.* **15,** 158 (1975).
5. R. von Helmolt, J. Wecker, B. Holzapfel, L. Schultz, and K. Samwer, *Phys. Rev. Lett*. **71,** 2331 (1993).
6. S. J. Schneider, R. S. Roth, and J. L. Waring, *J. Res. Natl. Bur. Stand., Sect. A* **65,** 345 (1961).
7. G. J. McCarthy, W. B. White, and R. Roy, *Mater. Res. Bull.* **4,** 251 (1969).
8. G. J. McCarthy, C. A. Sipe, and K. E. McIlvried, *Mater. Res. Bull.* **9,** 1279 (1974).
9. G. J. McCarthy, P. V. Gallagher, and C. A. Sipe, *Mater. Res. Bull.* **8,** 1277 (1973).
10. C. D. Brandle and H. Steinfink, *Inorg. Chem.* **8,** 1320 (1969).
11. H. L. Yakel and W. C. Koehler, *Acta Crystallogr*. **16,** 957 (1963).
12. S. Geller and E. A. Wood, *Acta Crystallogr*. **9,** 563 (1956).
13. P. Bordet, C. Chaillout, M. Marezio, Q. Huang, A. Santro, S.-W. Cheong, H. Takagi, C. S. Oglesby, and B. Batlogg, *J. Solid State Chem.* **106,** 253 (1993).
14. M. Marezio, J. P. Remeika, and P. D. Dernier, *Acta Crystallogr., Sect. B* **26,** 2008 (1970).
15. T. Shishido, K. Okamura, and S. Yajima, *J. Am. Ceram. Soc.* **61,** 373 (1978).
16. S. Geller, P. J. Curlander, and G. F. Ruse, *Mater. Res. Bull.* **9,** 637 (1974).
17. P. D. Dernier and R. G. Maines, *Mater. Res. Bull.* **6,** 433 (1971).
18. M. Marezio, J. P. Remeika, and P. D. Dernier, *Mater. Res. Bull.* **1,** 247 (1966).
19. M. Marezio, J. P. Remeika, and P. D. Dernier, *Inorg. Chem.* **7,** 1337 (1968).
20. T. Katsura, T. Sekine, K. Kitayama, T. Sugihara, and N. Kimizuka, *J. Solid State Chem.* **23,** 43 (1978).
21. N. Kimizuka, A. Yamamoto, H. Ohashi, T. Sugihara, and T. Sekine, *J. Solid State Chem.* **49,** 65 (1983).
22. I. Barin, "Thermochemical Data of Pure Substances." VCH Verlagsgesellshaft, Weinheim, Germany, 1989.
23. A. Navrotsky, *Phys. Chem. Miner*. **2,** 89 (1977).
24. A. Navrotsky, *Phys. Chem. Miner*. **24,** 222 (1997).
25. K. Leinenweber, J. A. Linton, A. Navrotsky, Y. Fei, and J. Parise, *Phys. Chem. Miner*. **22,** 251 (1995).
26. Y. Hu, A. Navrotsky, C.-Y. Chen, and M. E. Davis, *Chem. Mater*. **7,** 1816 (1995).
27. J. Liu, L. Topor, J. Zhang, A. Navrotsky, and R. C. Liebermann, *Phys. Chem. Miner*. **23,** 11 (1996).
28. I. Petrovic, P. J. Heaney, and A. Navrotsky, *Phys. Chem. Miner*. **23,** 119 (1996).
29. I. Kiseleva, A. Navrotsky, I. A. Belitsky, and B. A. Fursenko, *Am. Miner*. **81,** 658 (1996).
30. V. E. Lamberti, M. A. Rodriguez, J. D. Trybulski, and A. Navrotsky, *J. Mater. Res.* **11,** 1061 (1996).
31. L. Chai and A. Navrotsky, *Am. Mineral.* **81,** 1141 (1996).
32. S. Fritsch and A. Navrotsky, *J. Am. Ceram. Soc.* **79,** 1761 (1996).
33. H. Gan, M. C. Wilding, and A. Navrotsky, *Geochim. Cosmochim. Acta* **60,** 4123 (1996).
34. E. Takayama-Muromachi and A. Navrotsky, *J. Solid State Chem.* **106,** 349 (1993).
35. A. D. Shannon, *Acta Crystallogr., Sect. A* **32,** 751 (1976).
36. H. R. Hoekstra and K. A. Gingerich, *Science* **146,** 1163 (1964).
37. T. Atou, K. Kusaba, Y. Tsuchida, W. Utsumi, T. Yagi, and Y. Syono, *Mater. Res. Bull.* **24,** 1171 (1989).
38. J. P. Remeika and M. Marezio, *Appl. Phys. Lett*. **8,** 87 (1966).
39. F. Euler and J. A. Bruce, *Acta Crystallogr*. **19,** 971 (1965).
40. A. Navrotsky, *Geophys. Res. Lett*. **7,** 709 (1980).
41. A. Navrotsky, "Structure and Bonding in Crystals" (M. O'Keeffe and A. Navrotsky, Eds.), Vol. II. Academic Press, New York, 1981.
42. J. M. Neil, A. Navrotsky, and O. J. Kleppa, *Inorg. Chem.* **10,** 2076 (1971).
43. E. Ito, M. Akaogi, L. Topor, and A. Navrotsky, *Science* **249,** 1275 (1990).
44. J. L. Yarger, K. H. Smith, R. A. Nieman, J. Diefenbacher, G. H. Wolf, B. T. Poe, and P. F. McMillan, *Science* **270,** 1964 (1995).
45. H. R. Hoekstra, *Inorg. Chem.* **5,** 754 (1966).
46. D. T. Cromer, *J. Phys. Chem.* **61,** 753 (1957).
47. JCPDS 43-1015.
48. JCPDS 22-369.
49. JCPDS 21-579.
50. JCPDS 43-1029.
51. JCPDS 43-1008.

52. JCPDS 43-1014.
53. JCPDS 43-1006.
54. JCPDS 43-1036.
55. JCPDS 44-1268.
56. JCPDS 43-1007.
57. JCPDS 43-1034.
58. JCPDS 43-1037.
59. JCPDS 43-1021.
60. JCPDS 31-22.
61. M. Marezio, P. D. Dernier, and J. P. Remeika, *J. Solid State Chem.* **4,** 11 (1972).
62. JCPDS 8-147.
63. JCPDS 42-169.
64. JCPDS 32-16.
65. T. S. Chernaya, L. A. Muradyan, A. A. Rusakov, A. A. Kaminskii, and V. I. Simonov, *Kristallografiya* **30,** 72 (1985).
66. JCPDS 17-734.
67. JCPDS 12-758.
68. JCPDS 12-764.
69. JCPDS 14-128.
70. J. Sasvári and P.-E. Werner, *Acta Chem. Scand., Ser. A* **37,** 203 (1983).
71. JCPDS 13-426.
72. JCPDS 22-1108.
73. JCPDS 12-769.
74. JCPDS 23-589.
75. A. Kirfel and K. Eichhorn, *Acta Crystallogr., Sect. A* **46,** 271 (1990).
76. JCPDS 43-1013.
77. JCPDS 43-1012.
78. J. E. Weidenborner, *Acta Crystallogr.* **14,** 1051 (1961).
79. H. Huess, G. Bassi, M. Bonnet, and A. Delapalme, *Solid State Commun.* **18,** 557 (1976).
80. M. Bonnet, A. Delapalme, H. Huess, and M. Thomas, *Acta Crystallogr., Sect. B* **31,** 2233 (1975).
81. B. V. Kuvaldin, R. V. Bakradze, L. E. Fykin, and V. V. Martyshchenko, *Krystallografiya* **25,** 1155 (1980).
82. R. Diehl and G. Brandt, *Mater. Res. Bull.* **10,** 85 (1975).
83. J. C. Guitel, M. Marezio, and J. Mareschal, *Mater. Res. Bull.* **11,** 739 (1976).
84. M. Marezio and P. D. Dernier, *Mater. Res. Bull.* **6,** 23 (1971).
85. P. Coppens and M. Eibschütz, *Acta Crystallogr.* **19,** 524 (1965).